Adaptive ECMS based on speed forecasting for the control of a heavy-duty fuel cell vehicle for real-world driving

M. Piras [a], V. De Bellis [a], E. Malfi [a], R. Novella [b], M. Lopez-Juarez [b,*]

[a] *Industrial Engineering Department, Mechanic and Energetic Section, University of Naples "Federico II", via Claudio 21, 80125 Naples, Italy*
[b] *CMT-Motores Térmicos, Universitat Politècnica de València, Camino de vera s/n, 46022 Valencia, Spain*

ARTICLE INFO

ABSTRACT

Aiming at reducing pollutant emissions, hydrogen and fuel cell hybrid electric vehicles (FCVs) represent a promising technological solution. In this scenario, this paper proposes an adaptive energy management strategy (A-EMS) based on speed forecasting for a heavy-duty FCV, in order to achieve stable battery charge sustenance in realistic driving conditions. A validated and optimized fuel cell system model has been integrated into a complete vehicle model developed in the GT-Suite environment. A short-term velocity prediction layer based on a long short term memory (LSTM) neural network has been built in the A-EMS framework. The network has been trained and tested with realistic driving data simulated by GT-Real Drive for routes of the Trans-European Transport Network. The vehicle speed prevision has been realized over different forecasting horizons (5, 10, and 20 s). The adaptive equivalent consumption minimization strategy (A-ECMS) combined with short-term vehicle speed prediction is the A-EMS core algorithm of the presented work. Its results are here compared with the standard ECMS (S-ECMS) for four different driving cycles, including both standardized (HDDT) and realistic driving profiles. Three different European routes, with varying characteristics and from different countries, have been selected to test the proposed strategy in various conditions. The short-term prediction layer achieves satisfactory forecasting accuracy, with a RMSE ranging from 1.76 km/h to 13.37 km/h. The A-ECMS provides an improved by an order of magnitude battery charge sustenance, evaluated in terms of maximum battery state of charge (SoC) variation and fluctuation degree, with a hydrogen consumption increase ranging from 3.76% to 11.40% compared to the S-ECMS, for which the driving cycle is supposed to be known beforehand. As an example, in the HDDT cycle, the absolute maximum SoC variation and its fluctuation degree are lowered by about 76% and 79%, respectively. In conclusion, the proposed A-ECMS demonstrated that it is applicable for real driving conditions without prior knowledge of the driving cycle while improving battery charge sustaining for a FCV.

1. Introduction

In order to mitigate global warming, also caused by the high CO_2 emissions of the transport sector [1], a revolution of the transportation system with a lower carbon footprint is mandatory. Several countries are planning strategies to achieve this goal through fiscal incentives and regulations [2]. The European Union proposed a ban of internal combustion engine-powered vehicles supplied with fossil fuels starting from 2035 [3] and trucks manufacturers in Europe must reduce the CO_2 emissions of newly sold vehicles by 30% until 2030 compared to 2019 [4]. Even though hydrogen is not the only path to decarbonization, it is considered an essential option among a set of other technologies [5]. It has the advantage of being a versatile and clean energy vector acting as a buffer for renewable energy sources [6,7].

In this scenario, fuel cell powered vehicles (FCVs) represent a key technology for the automotive industry. Interest in them is constantly growing, as well as their market share [8]. Moreover, focusing on zero-emissions vehicles (ZEVs) in the heavy-duty sector, FCVs show several advantages when compared to battery electric vehicles (BEVs), mainly related to a higher driving range and a lower cost with a full pay-load [9]. As any relatively new technology, FCVs require deep research studies to optimize their architecture, performance, and maintenance. Further, because of their still high costs [10], simulations are even more important, especially in the design phases. Several fuel cell (FC) models have been proposed in the current literature [11–16] for FCVs studies, more focused on proton exchange membrane (PEM) fuel cells because of their low working temperature, silent operation, and rapid

starting. However, focusing on vehicular simulations to develop EMSs, even if the literature provides more detailed models [17], simplified approaches based on simple and constant polarization curves [18,19], simple polynomials [20,21], or a simplified fuel cell efficiency curve depending only on the fuel cell power [22,23] are preferred. These kinds of approaches can provide fast results with low computational effort compatible with an EMS. Moreover, in most of these studies the balance of plant (BoP) management was not optimized or the FC system was not validated, implying that results could be further improved. It is important to highlight that in the vehicle analysis, in addition to a reliable powertrain model, a proper energy management strategy (EMS) is required to handle the power distribution in complex powertrains with several energy sources, such as FCVs that usually include a lithium-ion battery coupled with the FC system. Rule-based strategies mainly depend on logical rules, based on feedback signals such as the battery state of charge (SoC) or the accelerator pedal position, and they are typically used in real-time applications thanks to their low computational effort, even though their control is not optimal [24–26]. Dynamic programming leads to optimal solutions and it is often taken to benchmark other strategies, however, it suffers from high computational load and cannot be applied for real-time control [27,28]. Pontryagin Minimum Principle (PMP) is classified as an online EMS that could be executed in real-time, providing results close to the optimal ones [29,30]. The main disadvantage is that results are strongly dependent on the initial co-state value. The Equivalence Consumption Minimization Strategy (ECMS) represents a simplification of the PMP in which co-state integration is no more required. ECMS control is close to optimal but its results highly depend on the equivalence factor value [31,32]. For the above-mentioned reasons, these strategies are not applied for real driving conditions without a proper real-time or iterative adaptation. Several approaches are proposed in the literature, such as fuzzy adaptive EMS (A-EMS) [33–35], feedback-based A-EMS [36,37] and forecasting enhanced control strategies [38,39]. In [40], Zhou et al. propose a multi-criteria power allocation strategy for a fuel cell/battery-based plug-in hybrid electric vehicle to enhance its operation efficiency. The strategy includes an adaptive online-learning enhanced Markov velocity-forecast approach, a state-of-charge reference planning approach, and a model predictive control approach. The results demonstrated a reduced hydrogen consumption by about 12%, but this methodology still presents some limitations. In fact, a series of standard driving cycles with different driving patterns (urban/suburban/highway) are concatenated to form the training dataset for the velocity predictor. A standard driving cycle, such as the HDDT, does not accurately represent real-world driving conditions because it is designed to be repeatable and standardized. Real-world driving patterns can vary greatly depending on factors such as traffic, weather, and driver behavior, which are not fully captured by standardized driving cycles. As a result, using a standard driving cycle as the basis for developing and testing vehicle predictive control strategies may not fully reflect the range of driving conditions that a vehicle is likely to encounter in real-world use. Moreover, the use of a fuel cell model based on a simple curve that relates fuel cell efficiency to current density represents an additional limitation. This model does not take into account the specific operating conditions of the fuel cell, such as temperature, pressure, fuel, and air composition. The work in [41] proposes a novel reinforcement learning-based energy management method for the fuel cell/lithium battery hybrid system. The proposed method can effectively reduce the life decay rate of fuel cells and improve fuel economy by up to 6% compared with other commonly used methods. In this case, as well, the fuel cell model is simplified and not validated with any experimental data. A multi-step Markov velocity predictor has been developed to predict vehicle speed. However, standard driving cycles constitutes the dataset for the velocity predictor training. Moreover, the EMS is also tested on a standard driving cycle (i.e. the WLTC), thus lacking verification of its performance under realistic driving conditions. In the Ref. [42] a

PMP-based A-EMS has been investigated, in which the co-state adaption was performed by driving cycle prediction. An improved Markov-based velocity prediction considering the driving behavior under different driving patterns was developed and the proposed A-EMS achieved a 4% reduction in hydrogen consumption compared to a rule-based strategy. Six different standard driving cycles were used as the dataset for the predictor configuration but they could not be representative of realistic driving conditions. Studies regarding applications of intelligent control strategies in realistic driving patterns are available in the present literature. However, they often refer to bus applications, where the road is repeated over time, lacking a verification for new and unknown driving conditions [43–45]. Sun et al. [46] proposed a real-time optimal EMS based on driving characteristics recognition for a bus application. The co-state for the PMP problem solution was forecasted in the following driving segment by a density-based spatial clustering of applications with noise algorithm, leading to a fluctuation range of SoC less than 2% and a hydrogen consumption reduced by 6.6% compared to a rule-based strategy. However, results have been obtained only for the selected and fixed bus routes.

1.1. Knowledge gaps

Considering the previous studies, the following conclusions can be extracted to provide an idea of the knowledge gaps in the literature about adaptive energy management strategy for fuel cell powered vehicles:

1. In most cases, driving cycle predictors, which are implemented in the control strategy, are trained and tested with standard driving cycles. Most of the standard driving cycles do not include driving patterns typical of transient real driving. In such a way, the A-EMS might not be suitable for realistic conditions [40,41, 47–50].
2. Most of the studies use low-order FC system models which are not validated or not previously optimized [40,41,49,51].
3. Studies that focus on realistic driving conditions usually deal with bus applications or cases with a fixed route, lacking verification for real driving conditions where the route is not known beforehand [43–46].
4. Studies on A-EMS for realistic conditions do not relate to heavy-duty FCV applications, so the performance of such vehicles with realistic control strategies in real driving conditions is unknown [52–54].

1.2. Contribution and objectives

Starting from the previous considerations, the main objective of this study is to develop an A-EMS for a fuel cell heavy-duty vehicle suitable for realistic applications fulfilling the knowledge gaps highlighted in the previous section. To achieve such an objective:

1. Realistic driving data have been generated by the GT-Real Drive tool [55] considering routes of the TEN-T [56] (Section 3.2). They have been then used to train a velocity predictor module, included in a complete A-ECMS (Section 5). Sensitivities analysis on the neural network parameters with realistic driving data confirmed that the proposed neural network achieved a prediction accuracy in line with the literature [43,51,57,58]. On the contrary to [40,41,47–51], the A-ECMS trained with realistic driving data applies to real-world driving and it is tested for one standard driving cycle (HDDT) and three realistic ones.
2. An FC system model validated at different operating conditions, that includes a fully optimized BoP, has been considered in this study (Section 2). Conversely to [40,41,47,50] the proposed model is able to consider the effects of the operating conditions on the fuel cell system efficiency and it is validated following the experimental data in [59,60]. The use of a more detailed model allows, as a future development, the possibility of incorporating a fuel cell degradation model.
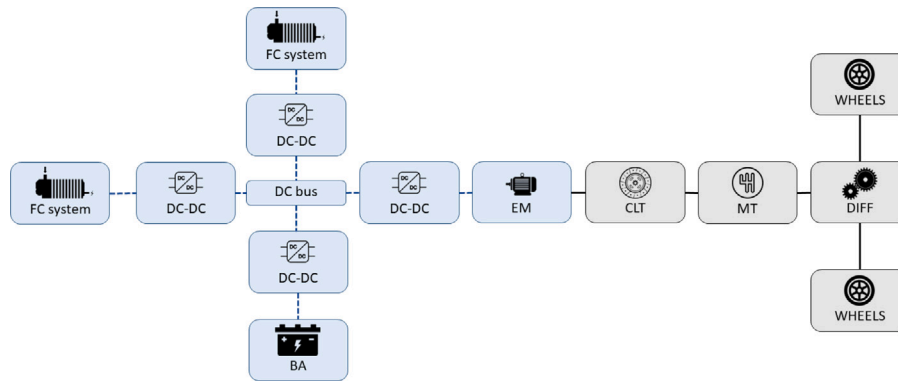
Fig. 1. Heavy-duty fuel cell hybrid electric vehicle powertrain scheme.

3. Relying on TEN-T roads, the EMS can be applied in any real driving condition, only requiring knowledge of the starting and ending points, and not only on a fixed and known set of repeatedly traveled roads, typical of bus applications.

4. This paper focuses on a heavy-duty fuel cell vehicle based on the Hyundai XCIENT FCV [61].

The scope of this paper does not only comprise the development of such tools but also their application and optimization to evaluate their performance and the comparison of the proposed A-ECMS to other energy management strategies in real driving conditions. Therefore, the novelty of this study can be attributed to the development of an A-ECMS trained with realistic driving data, hence applicable to real-world driving, capable of forecast the vehicle speed profile, its implementation and adaptation for a heavy-duty FCV, and the comparison of such an advanced A-ECMS with different forecasting horizons against a standard ECMS with the optimal equivalence factor. For this purpose, the following partial objectives are to be fulfilled:

- Integrate the A-ECMS in a full heavy-duty fuel cell vehicle.
- Identify the sensitivity of the prediction algorithm to the forecasting horizon length used for profile prediction.
- Evaluate the accuracy of velocity prediction of the algorithm in both standardized and realistic driving cycles.
- Analyze the SoC maximum variation with respect to the target value to identify whether this algorithm is suitable to prevent the battery from operating in degrading conditions.
- Determine a realistic range of values for the H_2 consumption for a heavy-duty fuel cell vehicle operated with a real-world EMS in real driving. Compare the change in performance against that obtained in standardized driving.

The results, discussed in detail in Section 5, demonstrate that the novelty of the paper lies in an A-EMS that, unlike the ECMS which requires offline calibration based on prior knowledge of the driving cycle, can be applied under realistic conditions by solely knowing the vehicle's starting and ending points while reducing fluctuations in the battery state of charge. Additionally, the proposed approach is based on realistic driving data, well-representative of driving conditions that could potentially be encountered on any route, unlike applications concerning fixed-route bus systems.

2. Simulation models

2.1. Vehicle model

In this study, a multi-FC system heavy-duty vehicle is adopted as the simulation model. The configuration of its powertrain is shown in Fig. 1.

Table 1
Main characteristics of the tested FCHEV, based on the Hyundai XCIENT FCV [61].

Fuel cell hybrid electric vehicle features	
Vehicle	
Mass (vehicle + cargo), kg	18 000
Car aero drag, m^2	9.38
Wheel diameter, m	0.468
Axle ratio, –	4.875
Fuel cell stacks	
Cells number, –	480
Max Power, kW	120
Max efficiency, –	0.62
DC-DC efficiency, –	0.95
Electric machine	
Max Power, kW	350
Max Torque, N m	3400
DC-DC efficiency, –	0.95
Battery	
Rated Capacity, Ah	110.55
DC-DC efficiency, –	0.95
Gearbox	
Gear 1 Ratio, –	4.484
Gear 2 Ratio, –	2.872
Gear 3 Ratio, –	1.842
Gear 4 Ratio, –	1.414
Gear 5 Ratio, –	1.000
Gear 6 Ratio, –	0.742

It consists of two fuel cell systems, a battery pack, DC-DC converters, an electric motor, a gearbox, and a differential. The main vehicle and components' characteristics are reported in Table 1. Similar to modern FCVs, the indirect electronic configuration has been selected to protect the FC systems from electric oscillations coming from the DC bus, also allowing the FC systems to be downsized. The vehicle model is implemented in the GT-Suite 2020 software. Concerning the electric machine, its efficiency has been estimated from a speed-torque map. The battery module calculates the state of charge of the battery pack, according to SoC-dependent internal resistance and open-circuit voltage. A deeper discussion about the fuel cell stack model is reported in the following section.

2.2. FC and BoP models

The fuel cell model was developed in previous authors' work [62, 63] and it is here briefly described. It includes both the fuel cell stack and all the BoP. Concerning the fuel cell, the relationship between its current density and the voltage is described by the polarization curve, defined by the following set of equations:

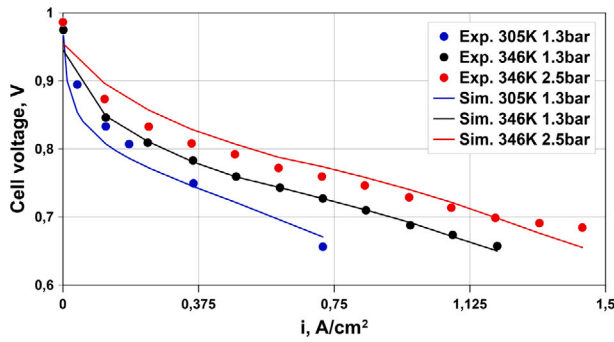$$V_{FC} = V_{OC} - V_{act} - V_{ohm} - V_{mt} \tag{1}$$

Fig. 2. Model/experiment comparison of cell voltage against current density for different cathode pressures and temperatures.

$$V_{OC} = \frac{-\Delta \bar{g}_f}{2F} \qquad (2)$$

$$V_{act} = \begin{cases} \frac{R_{gas}T}{2F}\left(\frac{i}{i_0}\right) \\ \frac{R_{gas}T}{2\alpha F} ln\left(\frac{i}{i_0}\right) \end{cases} \qquad (3)$$

$$V_{ohm} = R\,I \qquad (4)$$

$$V_{mt} = -C\,ln\left(1 - \frac{i}{i_l}\right) \qquad (5)$$

where V_{OC} is the open voltage circuit and V_{act}, V_{ohm} and V_{mt} are the activation, ohmic, and mass transport losses. The ohmic resistance R_{ohm} is modeled according to [64], taking into account the change in the ionic conductivity of the membrane as a function of the membrane water content, temperature, and membrane properties. The exchange current density depends on the FC temperature, the oxygen partial pressure, the electrochemical activation energy, the electrode roughness, and the reference exchange current density $i_{0,ref}$ [65]. GT-Suite genetic algorithms toolbox is used to calibrate the reference exchange current density, reference ohmic resistance, charge transfer coefficient (α), mass transport loss coefficient (C), limiting current density (i_l), and voltage open circuit losses values to validate the model at different conditions of pressure and temperature following the experimental data in [59,60]. The NSGA-III evolutionary global search genetic algorithm (GA) is selected as the optimization algorithm [66]. The optimization target for the GA was to minimize the overall error between the experimental and the simulation polarization curve voltage under different conditions of temperature and pressure. In order to ensure its convergence, 15 generations of solutions were used since after the 10–12 generations the error between the experimental and the simulation results evolution was asymptotic. The fuel cell model is validated by matching simultaneously three different numerical polarization curves, (for a total of 34 experimental points), to the experimental data under different conditions of temperature and pressure: $T_{cath} = 305$ K and $p_{cath} = 1.3$ bar, $T_{cath} = 346$ K and $p_{cath} = 1.3$ bar, $T_{cath} = 346$ K and $p_{cath} = 2.5$ bar. This validation procedure is a key point in driving cycle conditions, during which the fuel cell stack is subjected to different operating conditions depending on the external environment and BoP components operation. Synthetic validation results are shown in Fig. 2, where an overall RMS deviation between experimental data and model outcomes below 2% is obtained.

The fuel cell stack, whose main technical parameters are reported in Table 1, is integrated into a complete BoP model which was designed and optimized in a previous work [62]. It is composed of the complete anode and cathode circuits, their conditioning, and a cooling system, Fig. 3.

- The cathode side includes an e-charger compressor that supplies high-pressure air to the fuel cell stack, a heat exchanger that acts
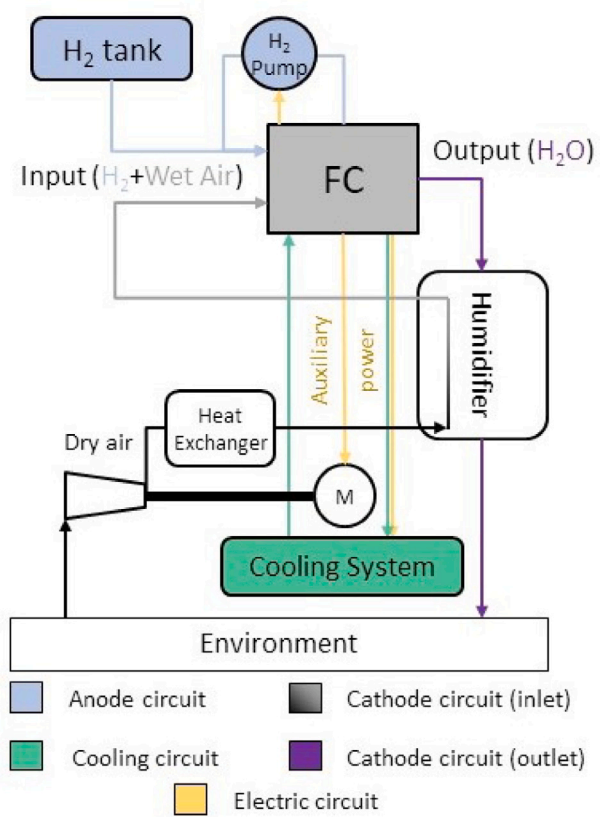

Fig. 3. Fuel cell system scheme.

as an intercooler, and a humidifier system that increases the cathode inlet relative humidity (RH) using the water available in the FC stack exhaust. The centrifugal compressor map is parametrized to meet the pressure and air mass flow rate requirements of the FC stack. Cathode stoichiometry and pressure are regulated using two PIDs, one controlling the power supplied to the e-charger and the other controlling the exhaust valve area. The heat exchanger is modeled with constant cooling efficiency of 70%, considering the coolant at 70 °C as the cold reservoir. The humidifier system is modeled using pipes connected by a thermal capacity to incorporate the effect of heat transfer. Water transport is modeled using water ejectors and injectors.
- The anode side comprises a 700 bar H_2 tank and an active H_2 recirculating loop powered by a pump. Anode pressure is regulated by controlling the valve connecting the recirculating loop and the H_2 tank, while anode stoichiometry is controlled using the pump powered by the FC.
- The cooling system consists of a cooling pump, powered by the FC, and a radiator to maintain the coolant temperature at 70 °C.

The main additional assumptions related to the BoP optimization are listed in the following:

- Due to the lack of data provided by Corbo et al. [59,60], cathode and anode pressure losses are modeled using data from the Ballard FCVelocity-9SSL fuel cell [67]. Membrane properties are listed in the Table 2.
- Cathode stoichiometry is fixed at 1.8 for a current density of 0.4 A/cm^2 or higher to avoid starvation during load changes;
- The relative humidity at the cathode inlet is targeted to 80% for every operating condition, provided that enough water from the cathode outlet can be extracted, and regulated by means of a PID controller following temperature and pressure variations;

Table 2
Fuel cell membrane main specifics.

Active surface area, cm^2	250
Membrane dry density, kg/m^3	3280
Membrane thickness, μ	189
Membrane dry equivalent weight, g/mol	1100

- Anode stoichiometry is 3 to avoid starvation and to increase the hydrogen diffusivity through the gas diffusion layer (GDL);
- The minimum cathode pressure is set as 1.2 bar to overcome the FC pressure losses;

In order to lower the overall vehicle simulation's computational effort, as done in [62], the FC model is simplified into a mean value model. Cathode pressure is identified as one of the most affecting variables influencing fuel cell performance and, for this reason, it is considered a fuel cell control variable together with the current, adding a certain level of dynamic to the model while increasing its accuracy.

3. Control algorithm

This paper proposes an adaptive EMS based on a long-short term memory neural network, with the aim of controlling a fuel cell range extender vehicle in real driving conditions that are unknown in advance. The control strategy is based on the hypothesis that the vehicle is equipped with a common GPS system to plan out the route to cover through a map service provider. This hypothesis is well-suitable for heavy-duty vehicles that usually connect defined points of interest such as airports, ports, and industrial areas. The additional assumption is that the vehicle certainly stops at every intersection or traffic light, whose relative position is evaluated by the map service provider. Under these hypotheses, the A-EMS can operate without any traffic information.

3.1. Equivalent consumption minimization strategy

The ECMS is chosen as the EMS core algorithm to ensure near the optimal local solution. It is the most known online EMS and it is based on the idea that electricity consumption can be converted into an equivalent amount of fuel. Power is then distributed minimizing the instantaneous equivalent fuel consumption that can be expressed as:

$$J = \dot{m}_f + s\frac{P_{batt}}{LHV} + \delta \tag{6}$$

where $\dot{m}_f$ and P_{batt} represent the actual fuel rate and the net electrical power as seen at the battery terminals, respectively, LHV and s are the lower heating value of the fuel and the equivalence factor, which represents the cost of the electric power drawn from the battery, and δ is a cost term to impose limitations on the fuel cells dynamic behavior. For this study, the function to be minimized is the H$_2$ consumption by realizing the optimal control that distributes power between the battery and the fuel cell systems while respecting the battery SoC charge-sustaining constraint. Exploring the effects of different levels of allowable dynamic for the fuel cell system (that affects membrane electrode assembly's degradation) is out of the scope of this work and, for this reason, a high limit on the current derivative with time ($|di/dt| \leq 0.1$ A/cm^2 s) is selected for all the test cases. This level of dynamics is high enough for the FC system to follow the e-motor power demand level with small support from the battery while avoiding undesired phenomena such as anode or cathode starvation that may lead to severe FC degradation [68]. The value of the equivalence factor is strongly dependent on the driving conditions and their a-prior knowledge is necessary to ensure the overall optimal control on the driving mission under the constraint of battery charge sustaining.

3.2. Velocity predictor

LSTM neural networks are a variant of recurrent neural networks with an additional memory component included to avoid the vanishing gradient problem to some extent. They have been widely adopted in research areas concerned with sequential data, such as text, audio, and video [69]. In complex time series prediction problems LSTM neural networks can adapt to multivariate and multi-input prediction problems where the classical linear method struggles [70]. The working principle of the LSTM cell can be described by its constituent elements: the input gate (i_t), forget gate (f_t), output gate (o_g), cell state (C_t), and hidden state (h_t). These gates and states can be mathematically represented as follows:

$$i_t = \sigma(W_{ig}[h_{t-1}, x_t] + b_{ig}) \tag{7}$$

$$f_t = \sigma(W_{fg}[h_{t-1}, x_t] + b_{fg}) \tag{8}$$

$$o_t = \sigma(W_{og}[h_{t-1}, x_t] + b_{og}) \tag{9}$$

$$\tilde{C}_t = tanh(W_c[h_{t-1}, x_t] + b_c) \tag{10}$$

$$C_t = f_t \odot C_{t-1} + i_t \odot \tilde{C}_t \tag{11}$$

$$h_t = o_t \odot tanh(C_t) \tag{12}$$

where W_{ig}, b_{ig} are weights, bias of input gate, W_{fg}, b_{fg} are weights, bias of forget gate, W_{og}, b_{og} are weights, bias of output gate, W_c, b_c are weights, bias of cell state, $\tilde{C}_t$ is the candidate cell state, σ denotes activation function, $\odot$ represents the scalar product of the two vectors. In Eq. (11), the input gate determines the amount of candidate cell state that is incorporated into the new cell state, while the forget gate determines whether to retain or discard the old cell state. By means of these gates, the LSTM architecture enables the selective addition (removal) of information to (from) the cell state. This mechanism empowers the LSTM to effectively mitigate the challenges posed by vanishing and exploding gradients, as the cell state can serve as an intermediary that preserves information from previous input and hidden states. Ultimately, the output gate provides the final output of the LSTM model. Based on the neural network architecture provided in [43], in this work, an LSTM neural network velocity predictor, composed of three LSTM layers with 128 neurons and one dense layer, is proposed. It is built in Matlab and its scheme is depicted in Fig. 4. The adaptive moment estimation (ADAM) optimizer, with a learning rate of 0.00611, is used to train the neural network. Sensitivities analysis on the neural network parameters with realistic driving data confirmed that the proposed neural network achieved a prediction accuracy in line with the literature [43,51,57,58]. More details are discussed in Section 5. The input sequence is composed of the historical series of three features: vehicle velocity, vehicle acceleration, and distance to the next intersection or traffic light. Owing to the information given by the map service provider, the distance can be evaluated as:

$$d_{jt} = \frac{D_j - \int_{t_j}^{t-t_j} v\,dt}{D_j}, t \in [t_j, t_{j+1}] \tag{13}$$

where d_{jt} is the distance feature from the intersection j to the intersection $j + 1$, D_j is the distance from the intersection j to the intersection $j + 1$, and t_j is the FCV arrival time at the intersection j. The historical sequence length (H_s) is fixed as 10 s while three different forecasting horizons (H_f) are considered, respectively 5, 10, and 20 s, to analyze their effects on the prediction accuracy and on the EMS. The network has been trained and tested with real driving data simulated by GT-Real Drive based on the TEN-T routes, where it is expected that the future heavy-duty FCV will operate. It is a tool of GT-Suite (Gamma Technologies) capable to generate routes along public roads worldwide from the map service provider MAPBOX while considering: live or historical traffic conditions, time of day and day of the week, traffic signals, driver preferences, and via points. The only required information is the vehicle starting position and its destination.
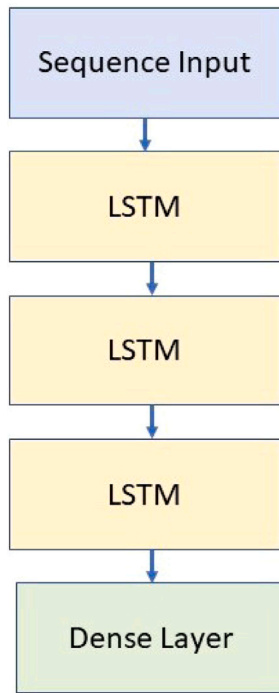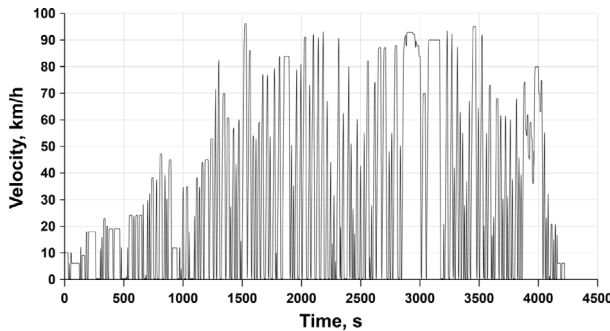
Fig. 4. Neural network architecture.

Fig. 5. Generated driving cycle in the route Napoli-Nola.

Table 3
TENT-T routes for the dataset generation.

Route	Country	Distance, km	Mean speed, km/h
Budapest-Tatabánya	Hungary	60	62.3
Fiumicino-Civitavecchia	Italy	71	67.4
Hamburg-Ahrensburg	Germany	34	27.9
Paris-Rouen	France	143	61.5
Siviglia-Algeciras	Spain	184	59.1
Ventspils-Riga	Latvia	184	36.7

Six different routes (Table 3) have been selected to generate the dataset, linking nodes of the TEN-T. The route selection for training and testing the EMS developed in this study is made considering very different speed profiles to prove the feasibility and adequacy of the present algorithm in any driving condition.

It is important to highlight that coupling GT-Real Drive with the TEN-T allows considering realistic driving information for important road corridors across Europe, realizing a reliable EMS for real heavy-duty vehicle applications. The dataset is standardized before training and 90% of the data is used for training and 10% for testing. As an example, the generated speed profile for the route Napoli-Nola used for testing is depicted in Fig. 5. To evaluate the accuracy of the velocity

Table 4
Pseudo code for the control algorithm.

Algorithm: ECMS based on speed forecasting
while (not terminate-condition)
%Short term velocity prediction layer
input: speed, acceleration and distance historical sequences;
$v_f(t+1, t+2, …, t+H_f)$ = NN prediction (input);
%Optimization layer
Optimize s in $[t; t+H_f]$;
%Bottom layer
Powertrain model + ECMS with s_{opt} for H_f seconds;
end

predictor on the testing data, the speed RMSE and R^2 are used as performance parameters. Their values are shown in Fig. 7.

As expected, the prediction accuracy decreases with the increase of the forecasting horizon. Nevertheless, the correlation between the predicted and the real data is in good agreement according to the values of R^2, being over 0.97 in the worst case. More detailed prediction results are reported in Section 5.

3.3. A-ECMS

The overall EMS scheme is represented in Fig. 6.

The control algorithm is fully developed in Matlab/Simulink while the vehicle simulation is performed by the GT-suite software. The co-simulation between the two platforms is established by the usage of the dedicated S-function Simulink block for GT-Suite models. A neural network-based adaptive ECMS is realized to overcome the ECMS limitations in unknown driving scenarios. The implementation of the A-ECMS can be divided into the offline design part and in the online application. The offline part includes the neural network design and training (previously discussed in Section 3.2). The online implementation is based on velocity forecasting, followed by equivalence factor optimization, and the consequent control sequence execution. In order to lower the computational effort of the EMS, the equivalence factor updating horizon length is set equal to H_f. For the sake of clarity, the EMS pseudo code is reported in Table 4.

4. Vehicle simulations

A set of four driving cycles, listed in Table 5, is selected to test the proposed A-ECMS. Four EMSs are analyzed: the standard ECMS with a constant and optimal equivalence factor that is taken as reference (S-ECMS for short) and the proposed A-ECMS with three different forecasting horizons of 5, 10, and 20 s (respectively A-ECMS-H5, A-ECMS-H10, A-ECMS-H20 for short). The HDDT cycle is chosen as the reference standard driving cycle, while the other test cases are representative of real driving conditions in Europe. They have been selected to explore different cases of route mean speed, travel distance, and for several European countries. The real driving cycles are generated by GT-Real Drive. It is important to point out that all four test cases are not part of the neural network training dataset, discussed in Section 3.2. Consequently, the A-EMS has been tested in the case of unknown driving conditions. The equivalence factor has been tuned for every test case in order to achieve the battery SoC sustaining for the S-ECMS. In compliance with range extender architectures, the initial SoC has been selected equal to 30%. The initial equivalence factor value for the A-ECMS is taken as the optimal one for the S-ECMS in the HDDT cycle for all the test cases. In such a way, unlike the S-ECMS, the A-ECMS does not require any offline tuning.
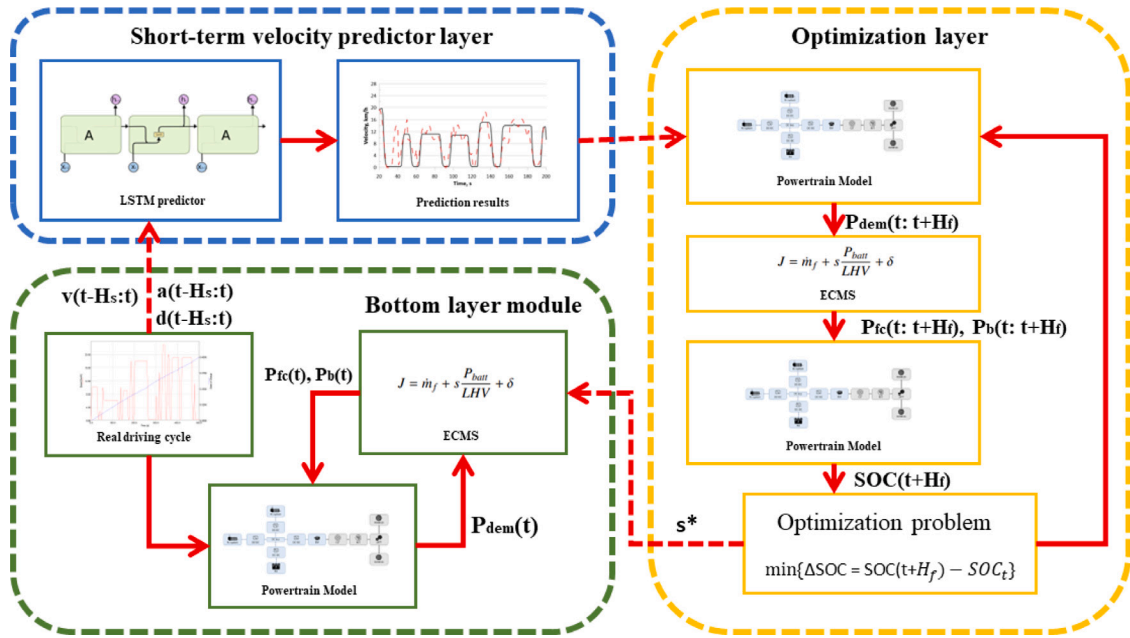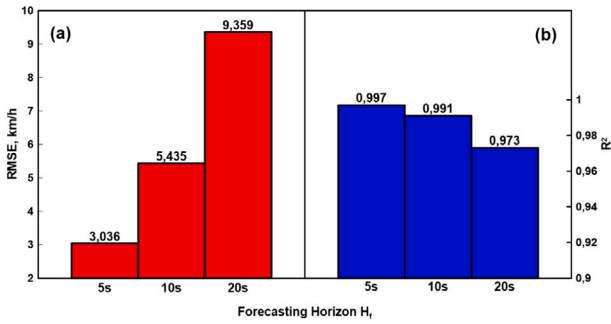
Fig. 6. Framework of the Adaptive-EMS.

Fig. 7. NN performance on the Test data: (a) velocity RMSE, (b) prediction R^2.

Table 5
Test cases definition based on TENT-T routes.

Route	Country	Distance, km	Mean speed, km/h
HDDT	–	37.2	64.2
Napoli-Nola	Italy	33.5	29.9
Strasburg-Metz	France	165.2	75.3
Bucarest-Giurgiu	Romania	62.3	39.4

5. Results and discussion

In this section, the results of the simulations described in Section 4 are analyzed. First, a detailed discussion of the HDDT case is carried out. In the second stage, the results in the cases of realistic driving cycles are analyzed in terms of speed prediction accuracy, battery SoC sustaining, and hydrogen consumption. The RMSE is used as the assessment parameter to evaluate the speed prediction accuracy, while maximum SoC (SoC_{max}), minimum SoC (SoC_{min}), maximum SoC variation ($\Delta = SoC_{max} - SoC_{min}$), and SoC RMSE, as expressed in Eq. (14), are reported to discuss the battery charge sustaining.

$$RMSE = \sqrt{\frac{\sum_{k=1}^{N}(SoC_k - SoC_{target})^2}{N}} \qquad (14)$$

The equivalent hydrogen consumption takes into account the difference between the initial and final energy of the battery (ΔE_b),

converted into an equivalent mass of hydrogen $H_{2,eq}$ as expressed by:

$$H_{2,eq} = H_2 + \frac{\Delta E_b}{\overline{\eta_b}\overline{\eta_{FCS}}LHV_{H_2}} \qquad (15)$$

where $\overline{\eta_b}$, $\overline{\eta_{FCS}}$ are the battery and FC systems efficiencies, respectively, while LHV_{H_2} is the hydrogen lower heating value.

Concerning the prediction accuracy, detailed results of the speed forecasting for the different H_f in the HDDT driving cycle are shown in Fig. 9 and in Fig. 10-a. The comparisons of Fig. 9-a-b-c point out that the three neural networks perform better in the fluctuation period, with greater errors in the acceleration and deceleration processes. The error increases with the lengthening of the forecasting horizon, as confirmed by the RMSE shown in Fig. 10-a. The last portion of the data highlights that the short-term velocity predictor layer is not able to accurately predict the restarts of the vehicle after a stop. However, the lower accuracy in the restart phases does not significantly affect the performance of the EMS. The RMSE values confirm a good agreement between the predicted speed and the real one for every forecasting horizon. Taking advantage of the predicted speed, the A-ECMS is able to improve the charge sustaining of the battery compared to the S-ECMS (Fig. 8, Table 6). The S-ECMS leads to a deeper battery discharge with a minimum SoC of 23.4% and a maximum SoC variation of 7.6%, which the A-ECMS-H5 can reduce by 76% reaching a maximum SoC variation of 1.7%. The SoC fluctuation for the A-ECMS is reduced for each forecasting horizon down to 79.54%, starting from an RMSE of 3.6% in the S-ECMS case down to less than 1% for the three A-ECMS variants. A more stable SoC has several advantages in real driving conditions without prior knowledge of the driving mission [42,71]. During the charge-sustaining mode, a fuel cell range extender vehicle (FCREx) works with a quite low battery SoC. Keeping the SoC around the target value allows for avoiding deep battery discharge that causes battery damage and degradation. On the other hand, in the A-ECMS cases, to reduce the SoC fluctuation, the FC system works more often in less efficient points, providing less power in the last portion of the driving cycle compared to the S-ECMS. In fact, even if during the last 500 s of the driving cycle the motor power request is low (Fig. 8-b), the S-ECMS selects higher fuel cell power to recover the deeper battery discharge while keeping the FC systems efficiency around 60%. On the contrary, the adaptive strategies do not require a battery SoC recovering and the FC system works at low power levels, satisfying
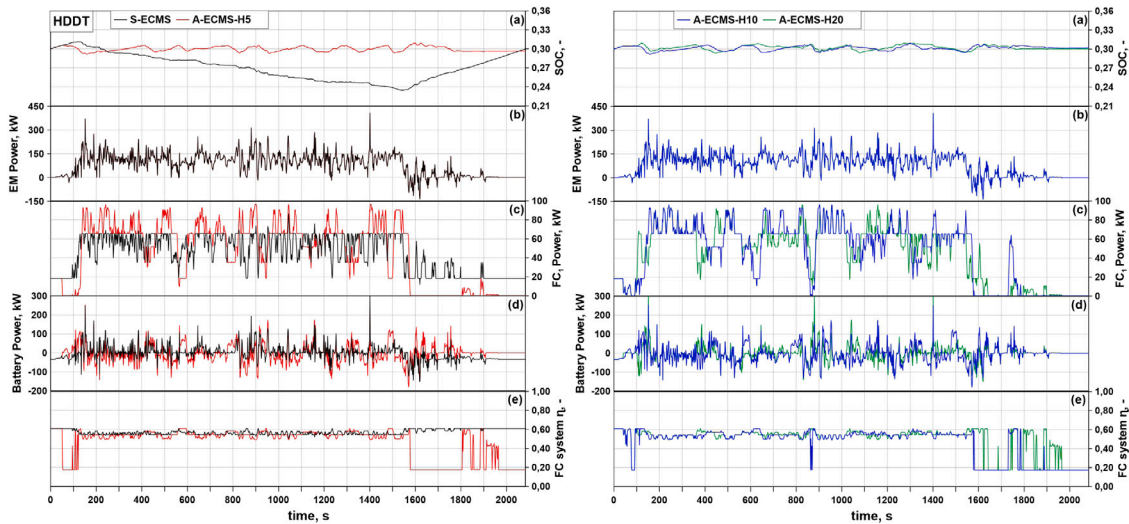
Fig. 8. HDDT, (a) S-ECMS/A-ECMS comparisons for different H_f of battery SoC, (b) Electric machine power, (c) Fuel cell system 1 net power, (d) Battery power and (e) and Fuel cell systems efficiency.
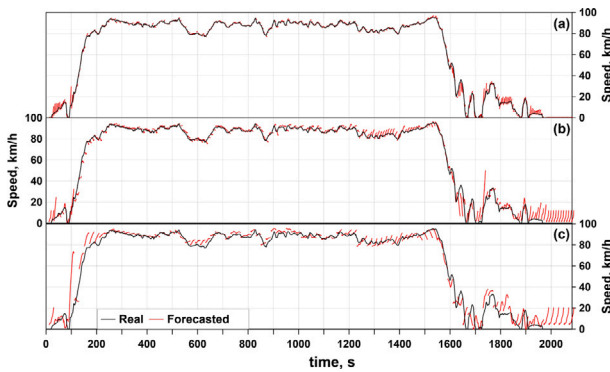

Fig. 9. Speed forecasting in the driving cycle HDDT for different forecasting horizons: (a) 5 s, (b) 10 s, (c) 20 s.
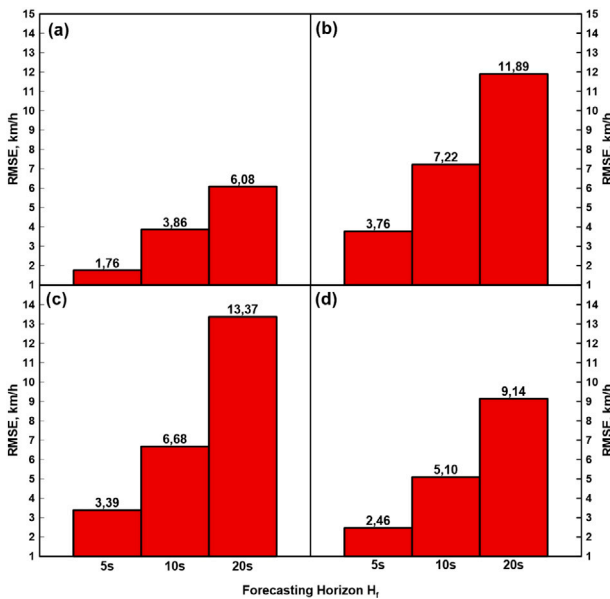

Fig. 10. RMSE for the forecasted speed comparisons for different forecasting horizons in the driving cycle: HDDT (a), Bucarest-Giurgiu (b), Napoli-Nola (c), Strasburgo-Metz (d).
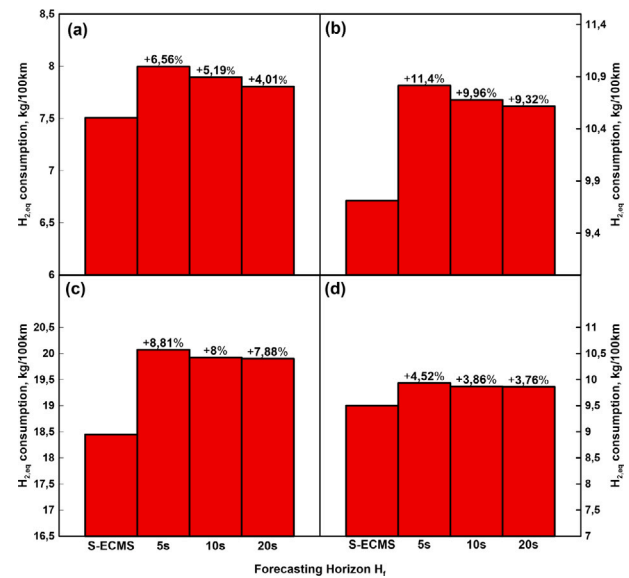

Fig. 11. H_2 consumption comparisons for different forecasting horizons in the driving cycle: HDDT (a), Bucarest-Giurgiu(b), Napoli-Nola (c), Strasburgo-Metz (d).

the power requested for traction. As a consequence, the equivalent hydrogen consumption is increased for the adaptive strategies (Fig. 11-a). The hydrogen consumption decreases with the increase of the forecasting horizon even if the forecasting accuracy is reduced. This is related to the reduction of the equivalence factor updating frequency. As explained in Section 3.2, the equivalence factor updating horizon length is set equal to the forecasting horizon. A greater updating frequency leads to more frequent load changes for the fuel cell systems, reaching very low current densities, characterized by lower efficiencies, when the battery SoC is above the target value, realizing continuous and inefficient fuel cell shutdowns.

The decrease of the speed forecasting accuracy while increasing the forecasting horizon is confirmed for all the analyzed test cases as evidenced in Fig. 10. The highest accuracy is realized by the A-ECMS-H5 for the HDDT cycle with an RMSE of 1.76 km/h, while the worst case is by the A-ECMS-H20 for the Napoli-Nola with an RMSE of 13.37 km/h. In each case, the prediction accuracy is in line with the current literature [43,51,57,58]. For the sake of simplicity, only the battery
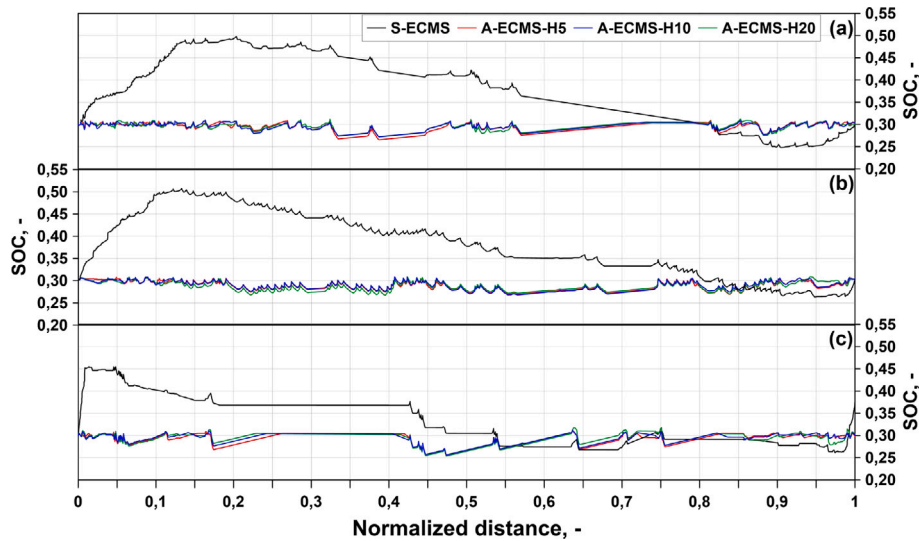
Fig. 12. S-ECMS/A-ECMS comparisons for different H_f of battery SoC for the real driving cycle: Bucarest-Giurgiu (a), Napoli-Nola (b), Strasburgo-Metz (c).

Table 6
SoC analysis for the tested strategies in the HDDT cycle.

Strategy	SoC_{min}, %	SoC_{max}, %	Δ, %	Difference, %	SoC RMSE, %	Difference, %
S-ECMS	23.45	31.09	7.64	–	3.64	–
A-ECMS-H5	29.17	30.91	1.74	−76.27	0.86	−77.22
A-ECMS-H10	29.19	30.91	1.72	−76.42	0.86	−77.51
A-ECMS-H20	29.38	30.94	1.56	−75.74	0.88	−79.54

Table 7
SoC analysis for the tested strategies in the Bucarest-Giurgiu road.

Strategy	SoC_{min}, %	SoC_{max}, %	Δ, %	Difference, %	SoC RMSE, %	Difference, %
S-ECMS	24.79	49.77	24.99	–	11.01	–
A-ECMS-H5	26.54	30.92	4.39	−89.30	1.18	−82.44
A-ECMS-H10	27.22	30.96	3.74	−90.19	1.08	−85.05
A-ECMS-H20	27.18	31.19	4.01	−90.03	1.10	−83.95

SoC evolution is depicted in Fig. 12 for the realistic driving cycles. The corresponding battery charge sustaining statistics are synthesized in Tables 7–9. The improved charge sustaining found for the HDDT cycle is here confirmed for the real driving missions. As an example, the Bucarest-Giurgiu route results are analyzed. In this case, the SoC RMSE lowers by 85% starting from 11.01% of the S-ECMS to 1.08% of the A-ECMS-H10. The maximum SoC variation is reduced too, from 24.99% of the S-ECMS to 3.74% of the A-ECMS-H10, realizing a reduction of 90.19%. It is relevant highlighting that the A-ECMS results are similar for all the considered forecasting horizons, showing the robustness of the proposed control algorithm. The highest S-ECMS SoC maximum variation is related to a high battery charging at the beginning of the simulation. In this case, reaching a SoC_{max} of 49.77% is not dangerous in terms of battery degradation, as opposed to a deep battery discharge, but this deviation from the target value is possible only because of the a-priori knowledge of the driving cycle. On the contrary, the A-ECMS selects the power distribution between the battery and the FC systems keeping the SoC almost constant without the knowledge of the future. This opens the possibility for a realistic implementation, where the planning of an optimal battery SoC trajectory requires a difficult long-term forecast and hence the EMS acts so to maintain the SoC to a target value, avoiding excessive SoC fluctuations and hence battery damage. However, because of the improved charge sustaining, sub-optimal solutions are found for the control problem by the A-ECMS, and the powertrain is forced to work with reduced efficiency, as shown by the higher equivalent hydrogen consumption for every test case (Fig. 11). Similar considerations can be made for the Napoli-Nola and the Strasburg-Metz routes.

6. Conclusion

This work proposes an A-ECMS compatible with real driving conditions for a heavy-duty FCV within the hypothesis that the vehicle is equipped with a common GPS system that knows in advance only the destination point of the driving mission. For this purpose, a complete powertrain model has been developed, incorporating a fully validated and optimized FC system model capable to reproduce physical phenomena in different boundary conditions. A short-term velocity prediction layer has been designed and integrated with the A-ECMS considering three different forecasting horizons. To this aim, realistic driving data has been collected by GT-Real Drive working with information from the TEN-T routes. The A-ECMS is compared with the reference S-ECMS for four different driving cycles, in terms of prediction accuracy, charge-sustaining statistics, and equivalent hydrogen consumption. The speed prediction accuracy decreases with the lengthening of the forecasting horizon. The A-ECMS-H5 achieves the highest accuracy for the HDDT cycle with an average RMSE of 1.76 km/h, while the worst case is by the A-ECMS-H20 for the Napoli-Nola with an RMSE of 13.37 km/h, which is in line with other studies in the literature [43,51,57,58]. The charge sustaining is improved both in terms of maximum SoC variations during the driving mission and fluctuation degree. As an example, in the Bucarest-Giurgiu route simulations the SoC RMSE is reduced by 85.05% for the A-ECMS-H10 compared to a value of 11.01% for the S-ECMS, while the maximum SoC variation is reduced by 90.19%. The A-ECMS provides an increase of hydrogen consumption for all the driving cycles, ranging from 3.76% to 11.40% compared to the S-ECMS However, the proposed A-EMS is feasible for realistic conditions, in

Table 8
SoC analysis for the tested strategies in the Napoli-Nola road.

Strategy	SoC_{min}, %	SoC_{max}, %	Δ, %	Difference, %	SoC RMSE, %	Difference, %
S-ECMS	26.33	50.75	24.42	–	11.37	–
A-ECMS-H5	26.89	30.74	3.84	−84.26	1.38	−87.87
A-ECMS-H10	26.77	30.85	4.07	−83.31	1.33	−88.27
A-ECMS-H20	26.99	30.93	4.24	−82.63	1.47	−87.05

Table 9
SoC analysis for the tested strategies in the Strasburg-Metz road.

Strategy	SoC_{min}, %	SoC_{max}, %	Δ, %	Difference, %	SoC RMSE, %	Difference, %
S-ECMS	26.09	45.47	19.37	–	6.64	–
A-ECMS-H5	25.57	31.19	5.62	−70.99	1.37	−79.45
A-ECMS-H10	25.61	31.07	5.47	−71.78	1.27	−80.94
A-ECMS-H20	25.34	31.77	6.43	−66.82	1.37	−79.40

which the driving cycle is not known a-priori, and improves the battery SoC sustaining, contributing to reducing the battery degradation. Future development includes the analysis of the effects of different fuel cell dynamic limitations on the EMS performance, taking into account the degradation of the fuel cell itself.

CRediT authorship contribution statement

M. Piras: Conceptualization, Investigation, Data curation, Formal analysis, Software, Methodology, Writing – original draft. **V. De Bellis:** Conceptualization, Supervision, Formal analysis, Writing – review & editing. **E. Malfi:** Supervision, Formal analysis, Writing – review & editing. **R. Novella:** Project administration, Resources, Data curation, Writing – review & editing. **M. Lopez-Juarez:** Investigation, Resources, Data curation, Methodology, Validation, Software, Writing – original draft.

Declaration of competing interest

The authors declare that they have no known competing financial interests or personal relationships that could have appeared to influence the work reported in this paper.

Data availability

Data will be made available on request.

Acknowledgments

References

[1] Road transport: EU-wide carbon dioxide emissions have increased by 24% since 1990.

[2] Slowik P, Hall D, Lutsey N, Nicholas M, Wappelhorst S. Funding the transition to all zero-emission vehicles. 2019.

[3] EU proposes effective ban for new fossil-fuel cars from 2035, https://www.reuters.com/business/retail-consumer/eu-proposes-effective-ban-new-fossil-fuel-car-sales-2035--2021-07-14/.

[4] Breed AK, Speth D, Plötz P. CO2 fleet regulation and the future market diffusion of zero-emission trucks in Europe. Energy Policy 2021;159:112640. http://dx.doi.org/10.1016/J.ENPOL.2021.112640.

[5] Fuel Cells, Undertaking HJ. Hydrogen roadmap Europe : a sustainable pathway for the European energy transition. Publications Office; 2019, http://dx.doi.org/10.2843/341510.

[6] Egeland-Eriksen T, Hajizadeh A, Sartori S. Hydrogen-based systems for integration of renewable energy in power systems: Achievements and perspectives. Int J Hydrogen Energy 2021;46:31963–83. http://dx.doi.org/10.1016/J.IJHYDENE.2021.06.218.

[7] Guilbert D, Yodwong B, Kaewmanee W, Phattanasak M. Power converters for hybrid renewable energy systems with hydrogen buffer storage: A short review. In: 6th IEEE international conference on smart grid, IcSmartGrids 2018. Institute of Electrical and Electronics Engineers Inc.; 2019, p. 28–33. http://dx.doi.org/10.1109/ISGWCP.2018.8634562.

[8] Samsun RC, Rex M, Antoni L, Stolten D. Deployment of fuel cell vehicles and hydrogen refueling station infrastructure: A global overview and perspectives. Energies 2022;15. http://dx.doi.org/10.3390/en15144975.

[9] Sagaria S, Moreira A, Margarido F, Baptista P. From microcars to heavy-duty vehicles: Vehicle performance comparison of battery and fuel cell electric vehicles. Vehicles 2021;3:691–720. http://dx.doi.org/10.3390/vehicles3040041.

[10] He X, Wang F, Wallington TJ, Shen W, Melaina MW, Kim HC, Kleine RD, Lin T, Zhang S, Keoleian GA, Lu X, Wu Y. Well-to-wheels emissions, costs, and feedstock potentials for light-duty hydrogen fuel cell vehicles in China in 2017 and 2030. Renew Sustain Energy Rev 2021;137:110477. http://dx.doi.org/10.1016/J.RSER.2020.110477.

[11] Shi W, Huangfu Y, Xu L, Pang S. Online energy management strategy considering fuel cell fault for multi-stack fuel cell hybrid vehicle based on multi-agent reinforcement learning. Appl Energy 2022;328:120234. http://dx.doi.org/10.1016/J.APENERGY.2022.120234.

[12] Wang X, Chen J, Quan S, Wang YX, He H. Hierarchical model predictive control via deep learning vehicle speed predictions for oxygen stoichiometry regulation of fuel cells. Appl Energy 2020;276:115460. http://dx.doi.org/10.1016/J.APENERGY.2020.115460.

[13] Quan S, Wang YX, Xiao X, He H, Sun F. Real-time energy management for fuel cell electric vehicle using speed prediction-based model predictive control considering performance degradation. Appl Energy 2021;304:117845. http://dx.doi.org/10.1016/J.APENERGY.2021.117845.

[14] Hu J, Wang Z, Du H, Zou L. Hierarchical energy management strategy for fuel cell/ultracapacitor/battery hybrid vehicle with life balance control. Energy Convers Manage 2022;272:116383. http://dx.doi.org/10.1016/J.ENCONMAN.2022.116383.

[15] Philip N, Ghosh PC. A generic sizing methodology for thermal management system in fuel cell vehicles using pinch analysis. Energy Convers Manage 2022;269:116172. http://dx.doi.org/10.1016/J.ENCONMAN.2022.116172.

[16] Zhou Y, Ravey A, Péra MC. Real-time cost-minimization power-allocating strategy via model predictive control for fuel cell hybrid electric vehicles. Energy Convers Manage 2021;229:113721. http://dx.doi.org/10.1016/J.ENCONMAN.2020.113721.

[17] Zhao J, Li X, Shum C, McPhee J. A review of physics-based and data-driven models for real-time control of polymer electrolyte membrane fuel cells. Energy AI 2021;6:100114. http://dx.doi.org/10.1016/j.egyai.2021.100114.

[18] Feng Y, Dong Z. Integrated design and control optimization of fuel cell hybrid mining truck with minimized lifecycle cost. Appl Energy 2020;270. http://dx.doi.org/10.1016/J.APENERGY.2020.115164.

[19] Gaikwad SD, Ghosh PC. Sizing of a fuel cell electric vehicle: A pinch analysis-based approach. Int J Hydrogen Energy 2020;45:8985–93. http://dx.doi.org/10.1016/J.IJHYDENE.2020.01.116.

[20] Wu X, Hu X, Yin X, Li L, Zeng Z, Pickert V. Convex programming energy management and components sizing of a plug-in fuel cell urban logistics vehicle. J Power Sources 2019;423:358–66. http://dx.doi.org/10.1016/J.JPOWSOUR.2019.03.044.

[21] Wu X, Hu X, Yin X, Peng Y, Pickert V. Convex programming improved online power management in a range extended fuel cell electric truck. J Power Sources 2020;476:228642. http://dx.doi.org/10.1016/J.JPOWSOUR.2020.228642.

[22] Ferrara A, Jakubek S, Hametner C. Energy management of heavy-duty fuel cell vehicles in real-world driving scenarios: Robust design of strategies to maximize the hydrogen economy and system lifetime. Energy Convers Manage 2021;232. http://dx.doi.org/10.1016/j.enconman.2020.113795.

[23] Fu Z, Zhu L, Tao F, Si P, Sun L. Optimization based energy management strategy for fuel cell/battery/ultracapacitor hybrid vehicle considering fuel economy and fuel cell lifespan. Int J Hydrogen Energy 2020;45(15):8875–86. http://dx.doi.org/10.1016/j.ijhydene.2020.01.017.

[24] Hames Y, Kaya K, Baltacioglu E, Turksoy A. Analysis of the control strategies for fuel saving in the hydrogen fuel cell vehicles. Int J Hydrogen Energy 2018;43:10810–21. http://dx.doi.org/10.1016/j.ijhydene.2017.12.150.

[25] Pam A, Bouscayrol A, Fiani P, Noth F. Rule-based energy management strategy for a parallel hybrid electric vehicle deduced from dynamic programming. In: 2017 IEEE vehicle power and propulsion conference, VPPC 2017 - proceedings, Vol. 2018-January. Institute of Electrical and Electronics Engineers Inc.; 2018, p. 1–6. http://dx.doi.org/10.1109/VPPC.2017.8331055.

[26] Zhu D, Pritchard E, Dadam SR, Kumar V, Xu Y. Optimization of rule-based energy management strategies for hybrid vehicles using dynamic programming. Combust Eng 2021;184:3–10. http://dx.doi.org/10.19206/CE-131967.

[27] Harselaar WV, Schreuders N, Hofman T, Rinderknecht S. Improved implementation of dynamic programming on the example of hybrid electric vehicle control. IFAC-PapersOnLine 2019;52:147–52. http://dx.doi.org/10.1016/J.IFACOL.2019.09.024.

[28] Wang Y, Jiao X. Dual heuristic dynamic programming based energy management control for hybrid electric vehicles. Energies 2022;15:3235. http://dx.doi.org/10.3390/EN15093235, 2022, Vol. 15, Page 3235.

[29] Ghasemi M, Song X. A computationally efficient optimal power management for power split hybrid vehicle based on pontryagin's minimum principle. In: ASME 2017 dynamic systems and control conference, DSCC 2017, Vol. 2. American Society of Mechanical Engineers Digital Collection; 2017, http://dx.doi.org/10.1115/DSCC2017-5244.

[30] Kang C, Song C, Cha S. A costate estimation for pontryagin's minimum principle by machine learning. In: 2018 IEEE vehicle power and propulsion conference, VPPC 2018 - proceedings. Institute of Electrical and Electronics Engineers Inc.; 2019, http://dx.doi.org/10.1109/VPPC.2018.8604982.

[31] Rezaei A, Burl JB, Zhou B. Estimation of the ECMS equivalent factor bounds for hybrid electric vehicles. IEEE Trans Control Syst Technol 2018;26:2198–205. http://dx.doi.org/10.1109/TCST.2017.2740836.

[32] Hegde S, Bonfitto A, Rahmeh H, Amati N, Tonoli A. Optimal selection of equivalence factors for ECMS in mild hybrid electric vehicles. In: Proceedings of the ASME design engineering technical conference, Vol. 1. American Society of Mechanical Engineers Digital Collection; 2021, http://dx.doi.org/10.1115/DETC2021-71621.

[33] Zhu Z, Zeng L, Chen L, Zou R, Cai Y. Fuzzy adaptive energy management strategy for a hybrid agricultural tractor equipped with HMCVT. Agriculture 2022;12:1986. http://dx.doi.org/10.3390/agriculture12121986.

[34] Shi D, Liu S, Cai Y, Wang S, Li H, Chen L. Pontryagin's minimum principle based fuzzy adaptive energy management for hybrid electric vehicle using real-time traffic information. Appl Energy 2021;286. http://dx.doi.org/10.1016/j.apenergy.2021.116467.

[35] Ravey A, Blunier B, Miraoui A. Control strategies for fuel-cell-based hybrid electric vehicles: From offline to online and experimental results. 2012, http://dx.doi.org/10.1109/TVT.2012.2198680.

[36] Onori S, Serrao L, Rizzoni G. Adaptive equivalent consumption minimization strategy for hybrid electric vehicles. In: ASME 2010 dynamic systems and control conference, DSCC2010, Vol. 1. 2010, p. 499–505. http://dx.doi.org/10.1115/DSCC2010-4211.

[37] Hussain S, Ali MU, Park GS, Nengroo SH, Khan MA, Kim HJ. A real-time bi-adaptive controller-based energy management system for battery–supercapacitor hybrid electric vehicles. Energies 2019;12:4662. http://dx.doi.org/10.3390/EN12244662, 2019, Vol. 12, Page 4662.

[38] Yang D, Wang L, Yu K, Liang J. A reinforcement learning-based energy management strategy for fuel cell hybrid vehicle considering real-time velocity prediction. Energy Convers Manage 2022;274:116453. http://dx.doi.org/10.1016/j.enconman.2022.116453.

[39] Han L, Jiao X, Zhang Z. Recurrent neural network-based adaptive energy management control strategy of plug-in hybrid electric vehicles considering battery aging. Energies 2020;13:202. http://dx.doi.org/10.3390/EN13010202, 2020, Vol. 13, Page 202.

[40] Zhou Y, Ravey A, Péra MC. Multi-objective energy management for fuel cell electric vehicles using online-learning enhanced Markov speed predictor. Energy Convers Manage 2020;213:112821. http://dx.doi.org/10.1016/J.ENCONMAN.2020.112821.

[41] Yang D, Wang L, Yu K, Liang J. A reinforcement learning-based energy management strategy for fuel cell hybrid vehicle considering real-time velocity prediction. Energy Convers Manage 2022;274:116453. http://dx.doi.org/10.1016/J.ENCONMAN.2022.116453.

[42] Li H, Ravey A, N'Diaye A, Djerdir A. Online adaptive equivalent consumption minimization strategy for fuel cell hybrid electric vehicle considering power sources degradation. Energy Convers Manage 2019;192:133–49. http://dx.doi.org/10.1016/J.ENCONMAN.2019.03.090.

[43] Zhang Z, He H, Guo J, Han R. Velocity prediction and profile optimization based real-time energy management strategy for plug-in hybrid electric buses. Appl Energy 2020;280. http://dx.doi.org/10.1016/j.apenergy.2020.116001.

[44] Xie S, Hu X, Xin Z, Brighton J. Pontryagin's minimum principle based model predictive control of energy management for a plug-in hybrid electric bus. Appl Energy 2019;236:893–905. http://dx.doi.org/10.1016/J.APENERGY.2018.12.032.

[45] Li M, Yan M, He H, Peng J. Data-driven predictive energy management and emission optimization for hybrid electric buses considering speed and passengers prediction. J Clean Prod 2021;304. http://dx.doi.org/10.1016/J.JCLEPRO.2021.127139.

[46] Sun X, Zhou Y, Zhang X, Huang L, Lian J. Real-time optimal EMS of adaptive charge sustenance for fuel cell hybrid buses based on driving characteristics recognition. Energy Convers Manage 2022;254. http://dx.doi.org/10.1016/j.enconman.2021.115192.

[47] Liu Y, Li J, Gao J, Lei Z, Zhang Y, Chen Z. Prediction of vehicle driving conditions with incorporation of stochastic forecasting and machine learning and a case study in energy management of plug-in hybrid electric vehicles. Mech Syst Signal Process 2021;158:107765. http://dx.doi.org/10.1016/j.ymssp.2021.107765.

[48] Li H, Ravey A, N'Diaye A, Djerdir A. Online adaptive equivalent consumption minimization strategy for fuel cell hybrid electric vehicle considering power sources degradation. Energy Convers Manage 2019;192:133–49. http://dx.doi.org/10.1016/j.enconman.2019.03.090.

[49] Zheng C, Zhang D, Xiao Y, Li W. Reinforcement learning-based energy management strategies of fuel cell hybrid vehicles with multi-objective control. J Power Sources 2022;543:231841. http://dx.doi.org/10.1016/j.jpowsour.2022.231841.

[50] Lee W, Jeoung H, Park D, Kim T, Lee H, Kim N. A real-time intelligent energy management strategy for hybrid electric vehicles using reinforcement learning. IEEE Access 2021;9:72759–68. http://dx.doi.org/10.1109/ACCESS.2021.3079903.

[51] Zeng T, Zhang C, Zhang Y, Deng C, Hao D, Zhu Z, Ran H, Cao D. Optimization-oriented adaptive equivalent consumption minimization strategy based on short-term demand power prediction for fuel cell hybrid vehicle. Energy 2021;227. http://dx.doi.org/10.1016/j.energy.2021.120305.

[52] Pulvirenti L, Rolando L, Millo F. Energy management system optimization based on an LSTM deep learning model using vehicle speed prediction. Transp Eng 2023;11:100160. http://dx.doi.org/10.1016/j.treng.2023.100160.

[53] Millo F, Rolando L, Tresca L, Pulvirenti L. Development of a neural network-based energy management system for a plug-in hybrid electric vehicle. Transp Eng 2023;11:100156. http://dx.doi.org/10.1016/j.treng.2022.100156.

[54] Zeng Y, Sheng J, Li M. Adaptive real-time energy management strategy for plug-in hybrid electric vehicle based on simplified-ECMS and a novel driving pattern recognition method. Math Probl Eng 2018;2018:5816861. http://dx.doi.org/10.1155/2018/5816861.

[55] GT-RealDrive - Gamma technologies, https://www.gtisoft.com/gt-realdrive/.

[56] TENtec interactive map viewer, https://ec.europa.eu/transport/infrastructure/tentec/tentec-portal/map/maps.html.

[57] Lin X, Wu J, Wei Y. An ensemble learning velocity prediction-based energy management strategy for a plug-in hybrid electric vehicle considering driving pattern adaptive reference SOC. Energy 2021;234. http://dx.doi.org/10.1016/j.energy.2021.121308.

[58] Han S, Zhang F, Xi J, Ren Y, Xu S. Short-term vehicle speed prediction based on convolutional bidirectional LSTM networks. 2019, p. 4055–60. http://dx.doi.org/10.1109/ITSC.2019.8917345.

[59] Corbo P, Migliardini F, Veneri O. Experimental analysis and management issues of a hydrogen fuel cell system for stationary and mobile application. Energy Convers Manage 2007;48:2365–74. http://dx.doi.org/10.1016/J.ENCONMAN.2007.03.009.

[60] Corbo P, Migliardini F, Veneri O. Experimental analysis of a 20 kWe PEM fuel cell system in dynamic conditions representative of automotive applications. Energy Convers Manage 2008;49:2688–97. http://dx.doi.org/10.1016/J.ENCONMAN.2008.04.001.

[61] FuelCellsWorks. World's first fuel cell heavy-duty truck, Hyundai XCIENT fuel cell, heads to Europe for commercial use. 2020.

[62] Molina S, Novella R, Pla B, Lopez-Juarez M. Optimization and sizing of a fuel cell range extender vehicle for passenger car applications in driving cycle conditions. Appl Energy 2021;285. http://dx.doi.org/10.1016/j.apenergy.2021.116469.

[63] Desantes JM, Novella R, Pla B, Lopez-Juarez M. Impact of fuel cell range extender powertrain design on greenhouse gases and NOX emissions in automotive applications. Appl Energy 2021;302. http://dx.doi.org/10.1016/j.apenergy.2021.117526.

[64] Springer TE, Zawodzinski TA, Gottesfeld S. Polymer electrolyte fuel cell model. 1991.

[65] Murschenhofer D, Kuzdas D, Braun S, Jakubek S. A real-time capable quasi-2D proton exchange membrane fuel cell model. Energy Convers Manage 2018;162:159–75. http://dx.doi.org/10.1016/J.ENCONMAN.2018.02.028.

[66] Deb K, Jain H. An evolutionary many-objective optimization algorithm using reference-point-based nondominated sorting approach, part I: Solving problems with box constraints. IEEE Trans Evol Comput 2014;18(4):577–601. http://dx.doi.org/10.1109/TEVC.2013.2281535.

[67] Abid R. Dynamic performance of a PEM fuel cell system. DTU Mech Eng 2013.

[68] Desantes J, Novella R, Pla B, Lopez-Juarez M. Effect of dynamic and operational restrictions in the energy management strategy on fuel cell range extender electric vehicle performance and durability in driving conditions. Energy Convers Manage 2022;266(X):115821. http://dx.doi.org/10.1016/j.enconman.2022.115821.

[69] Yu Y, Si X, Hu C, Zhang J. A review of recurrent neural networks: Lstm cells and network architectures. Neural Comput 2019;31:1235–70. http://dx.doi.org/10.1162/neco_a_01199.

[70] Hochreiter S, Schmidhuber J. Long short-term memory. Neural Comput 1997;9:1735–80. http://dx.doi.org/10.1162/NECO.1997.9.8.1735.

[71] Li H, Ravey A, N'Diaye A, Djerdir A. A novel equivalent consumption minimization strategy for hybrid electric vehicle powered by fuel cell, battery and supercapacitor. J Power Sources 2018;395:262–70. http://dx.doi.org/10.1016/J.JPOWSOUR.2018.05.078.